University of Reading

School of Mathematical and Physical Sciences

Fast Diffusion in Porous Media

Justin Prince

August 2011

This dissertation is for a joint MSc in the Departments of Mathematics & Meteorology and is submitted in partial fulfilment of the requirements for the degree of Master of Science.

Abstract

This dissertation is concerned with the flow of chemical agents through porous media at low levels of saturation, giving rise to a fast diffusion process. A velocity based moving mesh method based upon the assumption of local mass conservation is applied to the porous medium equation in one dimensional cartesian and radial coordinates and discretised using both finite differences and finite elements. Comparisons are drawn between the fast and slow diffusive regimes, evaporation is also considered from the domain. An appropriate numerical model output in three dimensions is successfully compared to some real experimental data.

Acknowledgements

I would like to thank my supervisors, Professor Mike Baines and Doctor Alex Lukyanov for their help and advice during the course of this dissertation. I'd also like to thank the Natural Environmental Research Council for their financial support throughout this year.

Declaration

I confirm that this is my own work and the use of all material from other sources has been properly and fully acknowledged.

Signed .....

Chapter 1

Introduction

This dissertation is concerned with the application of moving meshes applied to nonlinear diffusion, specifically the porous medium equation. We shall discuss a conservation based moving mesh method based on advecting the nodes with the fluid velocity. In particular this method will be applied to modelling the dispersion of liquid chemicals in the porous medium (otherwise known as the fate of chemical agents).

1.1 Background

Exposure to chemical agents can have a major impact on the environment. Being able to model the fate of the agent accurately is therefore an extremely useful tool.

When a chemical agent is released into a porous medium, diffusion will occur and the substance will spread. The rate of diffusion depends, among other factors, on the properties of the medium as well as those of the chemical agent. To model the diffusive properties of the medium, features such as the size and coarseness of grains are considered. Also, when modelling the chemical agent, properties such as the viscosity and the temperature at which it vaporizes are important.

It is well known that a spreading liquid in a porous medium can form a capillary

bridge network, which aids the di usive process. As described in [11], at very low levels of saturation the liquid bridges between grain particles are only connected by the thin lms covering grain particles, see gure 1.1. These low levels of saturation cover a wide range of values, so understanding the change in transport properties of the medium at these levels is of vital importance. The network properties are de ned by the di usive regime imparted by these conditions.

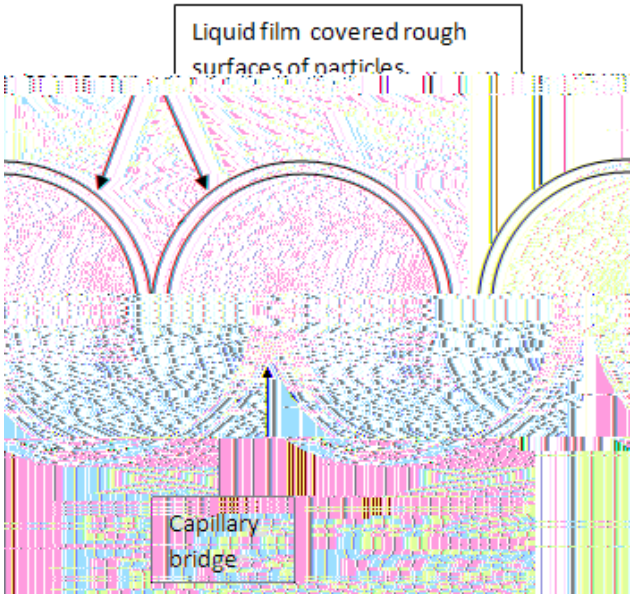

Figure 1.1: Schematic to show two grains within a porous medium at low levels of saturation

Capillary transport at low levels of liquid saturation is generally a slow process compared to di usion at higher levels of liquid saturation [4], but it is the process responsible for the long term distribution and therefore for environmental e ects.

In the situation where saturation levels are low a process can occur referred to in modelling terms as fast di usion. The features that distinguish this fast di usion regime from normal or slow di usion are that the liquid is only contained in isolated capillary bridges and on the rough surface of particles.

properties of the porous medium equation.

We split Chapter 3 into two main sections for modelling di usion by the porous medium equation which (i) excludes and (ii) includes evaporation. (i) In this rst section we have the property of local mass conservation. This allows us to derive a Lagrangian velocity-based moving mesh method. This essentially takes an initial mesh and advects the nodes at the Darcy velocity using local mass conservation, allowing the solution to evolve with the mesh. (ii) In the second section we no longer have mass conservation because we include evaporation into the di usion process. This requires us to take a slightly di erent approach whereby local mass fractions are conserved. Both approaches are implemented in both 1D Cartesian and d-dimensional radially symmetric coordinates. We begin modelling in 1D Cartesian coordinates since the procedure is clearer in that case. The key coordinate system for comparing the numerical model to the experimental data will be radially symmetric in 3D, allowing us to capture the hemispheric geometry of the di using chemical agent.

We end with Chapter 6 where we conclude our findings and suggest avenues for further work in this field.

Apart from the comparison between the numerical model with some experimental data, in Chapter 5 we will not be concerned with precise physical values. Instead we shall use values that are representative of the phenomena that we expect to see.

(i) Mass

Also known as the continuity equation, the equation of mass conservation is given by

$$_t + r \quad (\quad V) = 0 \tag{2.2}$$

where $\quad 2 (0; 1)$ is the porisity of the medium, V is the velocity, r is the divergence operator, and $\quad$ is the density.

(i) Darcy's Law

Darcy's Law is generally used to describe the dynamics of ows through porous media and is given by

$$V = \quad r \; p \tag{2.3}$$

where p is the pressure of the gas, $\quad$ is the viscosity and $\quad$ is the permeability tensor which we take to be a constant.

(i) Equation of State

An equation of state for a uid is the ideal gas law

$$p = p_0 \tag{2.4}$$

where p_0 is some chosen reference pressure and $\quad 1$ is the speci c heat ratio.

To form the PME (2.1), we rst substitute (2.4) into (2.3) to give

$$\begin{aligned} V &= \quad -r \; p_0 \\ &= \quad \frac{p_0}{\quad} r \\ &= \quad \frac{p_0}{\quad} \quad {}^1 r \quad ; \end{aligned} \tag{2.5}$$

which can then be substituted into (2.2) to give

$$_t = \frac{p_0}{\quad} r \quad (\quad r \quad): \tag{2.6}$$

By writing = u and = m and scaling out the constant $\frac{p_0}{}$ we arrive at the PME (2.1).

2.2 [illegible]

We also want to study the e ects of evaporation by the introduction of a negative source term in (2:1), arising from mass balance. The PME with a source term is known as the CPME [17] and takes the form

$$u_t = r \quad (u^m r \ u) + s(x) \tag{2.7}$$

where s(x) is the source term.

2.3 [illegible]

Due to the physical nature of the problem discussed in x1.1, we have a Dirichlet boundary condition and zero total ux at the moving boundary i.e.

$$u = u_b \text{ and } uv + u^m r \ u\,\hat{n} = 0; \tag{2.8}$$

where $\hat{n}$ is the normal to the boundary and we choose $u = u_b$ to be a small fraction of the total initial value of u. This represents the threshold value beyond which the capillary network bridges of uid between granules of the porous media break, as described in x1.1.

In the standard PME problem u = 0 on the boundary, although putting $u \neq 0$ removes one of the di culties of the equation since the standard PME is degenerate at u = 0. A consequence is that waiting times do not arise in this problem.

We also assume an initial data function

$$u(x;0) = u^0(x) \tag{2.9}$$

2.4 [illegible]

A property of the PME (2.1) with the boundary conditions (2.8) is conservation of mass, which we now verify using similar methods to those in [3]. For a region (t) with a boundary @ (t) moving with the normal velocity vn^ we begin by di erentiating the total mass integral with respect to time and applying Reynolds Transport Theorem [18], so that

$$\frac{d}{dt}\int_{(t)} u\,dx = \int_{(t)} u_t\,dx$$

The 1D Cartesian form of (2.1) is

$$u_t = \frac{@}{@x}\ u^m \frac{@u}{@x}\ ; \tag{2.14}$$

with moving boundaries at a(t) and b(t), which will be solved on a moving mesh $x_i(t)$, for $i = 0; :::N$, such that

$$a(t) = x_0(t) < x_1(t) < ::: < x_{N\ 1}(t) < x_N(t) = b(t) \tag{2.15}$$

The boundary conditions are

$$u = u_b \ \text{ and } \ uv + u^m u_x = 0 \ \text{ at } \quad x(t) = a(t); b(t); \quad t > 0; \tag{2.16}$$

which are equivalent to the multi-dimensional boundary conditions (2.8).

The one dimensional version of the initial data (2.9), for (2.14) is

$$u(x; 0) = u^0(x) \tag{2.17}$$

in the region $x_i(t^0)\ 2\ [a(t^0); b(t^0)]$. From (2.17), we choose

the entire domain which in the case of $d = 1; 2$ is the whole domain, consistent with the physical problem. However in the case $d = 3$ modelling evaporation in this way becomes invalid as it only occurs over the boundary.

The change in boundary conditions and initial data from Cartesian to radial coordinate systems is a trivial alteration from (2.16) and (2.17) respectively.

Chapter 3

A Lagrangian method

In this chapter we describe a Lagrangian approach used to design a moving mesh method for the PME. The idea of the method is to use the principle of local mass conservation to generate a velocity with which to advance the mesh. When dealing with a mass conserving problem the velocity based moving mesh method is consistent with the total integral of the density being constant. We initially look at the mass conserving problem where there is no evaporation occuring and then at the non-mass conserving evaporation case. In both cases we go on to show how the solution u can be recovered algebraically from the new mesh and the constant masses using conservation properties.

3.1 Derivation of the velocity

We shall describe the method to generate the velocity of the nodes from the local mass conservation principle for both the 1D Cartesian case and the radially symmetric case in d dimensions.

3.1.1 Method

Here we consider the PME (2.14) in one dimension, with zero flux and $u = u_b$ on the boundaries. We know that the total mass is conserved from equation (2.13) which in 1D is

$$\int_0^{b(t)} u\,dx = c \tag{3.1}$$

For local mass to be conserved we require it to be constant for all time. The mass from 0 to a general point $\hat{x}_i(t)$ in $(0; b(t))$ is

$$\int_0^{\hat{x}_i(t)} u\,dx = c_i \tag{3.2}$$

for $u > 0$. We assume that the $\hat{x}_i(t)$ are such that the c_i's are constant in time, corresponding to mass conservation in the segment from 0 to $\hat{x}_i(t)$.

We now differentiate (3.2) with respect to time and apply Leibnitz' integral rule to find that

$$\frac{d}{dt}\int_0^{\hat{x}_i(t)} u\,dx = \int_0^{\hat{x}_i(t)} \frac{\partial u}{\partial t}\,dx + \left[u\frac{dx}{dt}\right]_0^{\hat{x}_i(t)} \tag{3.3}$$

Substituting from (2.14) we have

$$\begin{aligned}
\frac{d}{dt}\int_0^{\hat{x}_i(t)} u\,dx &= \int_0^{\hat{x}_i(t)} \frac{\partial}{\partial x}\left(u^m \frac{\partial u}{\partial x}\right) dx + \left[u\frac{dx}{dt}\right]_0^{\hat{x}_i(t)} \\
&= \left[u^m \frac{\partial u}{\partial x} + u\frac{dx}{dt}\right]_0^{\hat{x}_i(t)} \\
&= \left[u\left(u^{m-1}\frac{\partial u}{\partial x} + \frac{dx}{dt}\right)\right]_0^{\hat{x}_i(t)} \\
&= u\left(u^{m-1}\frac{\partial u}{\partial x} + \frac{dx}{dt}\right)_{x=\hat{x}_i(t)} = 0
\end{aligned} \tag{3.4}$$

using the assumption that the c_i's in (3.2) are constants. We note that (3.4) is equivalent to zero total flux through all segment boundaries. We can now rearrange (3.4) to give the velocity at any point $\hat{x}_i(t)$ as

$$v_i = \frac{dx_i}{dt} = -u_i^{m-1}\left(\frac{\partial u}{\partial x}\right)_i = -\frac{1}{m}\left(\frac{\partial}{\partial x}(u^m)\right)_i \tag{3.5}$$

provided that $u_i \neq 0$. So we know that in order to preserve mass we must move nodes with this velocity. We notice at this point that the velocity (3.5) is that arising from Darcy's Law (2.3).

3.1.2 The Finite Difference Method

In the finite difference method (3.5) is approximated by

$$v_i = \frac{dx_i}{dt} = \frac{1}{m} \frac{\left(u_{i+1}^n\right)^m - \left(u_{i-1}^n\right)^m}{x_{i+1}^n - x_{i-1}^n} \tag{3.6}$$

To obtain the new mesh from (3.6) we employ explicit Euler timestepping, as in

$$\frac{x_i^{n+1} - x_i^n}{\Delta t} = \frac{1}{m} \frac{\left(u_{i+1}^n\right)^m - \left(u_{i-1}^n\right)^m}{x_{i+1}^n - x_{i-1}^n}; \tag{3.7}$$

taking the values of x_i and u_i on the right hand side at the previous time level n. A stability condition on Δt is required, in addition to which there is a condition to prevent node overtaking also required. To do the latter we impose in effect a Lagrangian type CFL condition on the scheme, limiting the size of the timestep that we can take relative to the size of the space step such that for a general point x_i

$$|(v_{i+1} - v_i)\,\Delta t| < |x_{i+1} - x_i|, \quad \forall i, t \tag{3.8}$$

The condition (3.8) may not guarantee stability of (3.7), but by following this restriction we can prevent nodes overtaking. In practice the value of Δt is estimated by trial and error.

Conservation tells us that the c_i's in (3.2) remain constant for all time. This tells us that for a general point $\hat{x}_i(t)$ we have

$$\int_{\hat{x}_{i-1}(t^{n+1})}^{\hat{x}_{i+1}(t^{n+1})} u(x, t^{n+1}$$

where the c_i's are from (3.2).

3.1.3 Semi-implicit timestepping

We now describe a semi-implicit timestepping method for finding the nodal position. This is useful because it allows us to take a longer timestep than with an explicit method and also prevents nodes overtaking. This method is still first order in time but avoids the Lagrangian type CFL condition (3.8), allowing larger timesteps to be taken.

We begin with a form of the scheme (3.7) for the nodal velocity formulated in 3.1.2, taking $m = 1$ for clarity. We can write

$$\frac{x_i^{n+1} \quad x_i^n}{t} = \quad u_{i+1}^n$$

for (1 i N 1), where

$$e_i^n = \frac{u_{i+\frac{1}{2}}\ t}{x_i^n\ x_{i\ 1}^n\ x_{i+\frac{1}{2}}^n\ x_{i\ \frac{1}{2}}^n}$$

$$f_i^n = 1 + \frac{u_{i\ \frac{1}{2}}\ t}{x_{i+1}^n\ x_i^n\ x_{i+\frac{1}{2}}^n\ x_{i\ \frac{1}{2}}^n} + \frac{u_{i+\frac{1}{2}}\ t}{x_i^n\ x_{i\ 1}^n\ x_{i+\frac{1}{2}}^n\ x_{i\ \frac{1}{2}}^n}$$

$$g_i^n = \frac{u_{i\ \frac{1}{2}}\ t}{x_{i+1}^n\ x_i^n\ x_{i+\frac{1}{2}}^n\ x_{i\ \frac{1}{2}}^n}$$

We can now determine x_i^{n+1} by inverting the tridiagonal matrix on the left hand side of the following tridiagonal system

$$\begin{matrix} 0 & & & & \\ f_1^n & g_1^n & 0 & \cdots & 0 \\ e_2^n & f_2^n & g_2^n & \cdots & 0 \\ \vdots & \ddots & \ddots & \ddots & \vdots \\ 0 & \cdots & e_{N\ 2}^n & f_{N\ 2}^n & \end{matrix}$$

08.293 3.064 Td [( )]TJ/F25 11.9552 Tf 11.955 0 Tf

3.1.4 Burgers

The radially symmetric porous medium equation (2.18) is

$$\frac{\partial u}{\partial t} = \frac{1}{r^{d-1}} \frac{\partial}{\partial r} \left(r^{d-1} u \right)$$

since the c_i's are constants. As before this is equivalent to zero total flux through all section boundaries.

We can rearrange (3.23) to find the velocity as in §3.1.1, giving

$$v_i = \frac{dr_i}{dt} = u_i^{m-1} \left.\frac{\partial u}{\partial r}\right|_i = \frac{1}{m} \left.\frac{\partial}{\partial r}(u^m)\right|_i \tag{3.24}$$

Once again, as would expected for a mass conserving problem, we have derived the Darcy velocity as in (3.5) except in terms of the radial coordinate.

In the finite difference method using radially symmetric coordinates (3.24) is approximated as

$$v_i = \frac{dr_i}{dt} = \frac{1}{m} \frac{\left(u_{i+1}^n\right)^m - \left(u_{i-1}^n\right)^m}{r_{i+1}^n - r_{i-1}^n}; \tag{3.25}$$

and to find the new nodal positions $r_i(t)$ we use explicit Euler timestepping as in §3.1.2, or semi-implicit timestepping as in §3.1.3.

Due to the conservation in each section we can use the new mesh spacing to recover the solution u, as in (3.10), which in the radial sense is

$$u_i(r; t^{n+1}) = \frac{c_{i+1} - c_{i-1}}{r_i^{d-1}(t^{n+1})\left(r_{i+1}(t^{n+1}) - r_{i-1}(t^{n+1})\right)} \tag{3.26}$$

3.2 Including evaporation

In the remainder of the chapter we consider the evaporation case, as described physically in §1.1. In this case global mass conservation no longer applies. This requires us to take a slightly different approach to finding the nodal velocity, this time based on local conservation of mass fractions.

As in §3.1 we first describe the method to find the velocity in 1D Cartesian coordinates and then generalise to radially symmetric coordinates in d dimensions (although $d = 2$ is the only realistic value physically).

3.2.1 Evaporation

We consider the CPME (2.7) with evaporation from the boundary in one dimension. A source term is present and for now we shall keep the general form s(x) so that

$$u_t = \frac{\partial}{\partial x}\left(u^m \frac{\partial u}{\partial x}\right) + s(x) \tag{3.27}$$

where in practice s(x) is negative. Evaporation will cause total the mass to reduce, eventually to zero and local mass cannot be conserved. We therefore require another way to derive the velocity. Let us define the total mass to be

$$\int_0^{b(t)} u\,dx = \alpha(t); \tag{3.28}$$

say, which now varies with time. Taking the time derivative of (3.28) using Leibnitz Integral Rule we find that

$$\begin{aligned} \alpha'(t) &= \frac{d}{dt}\int_0^{b(t)} u\,dx \\ &= \int_0^{b(t)} u_t\,dx + [uv]_0^{b(t)} \end{aligned} \tag{3.29}$$

Substituting in (3.27) we have

$$\begin{aligned} \alpha'(t) &= \int_0^{b(t)} \left[\frac{\partial}{\partial x}\left(u^m \frac{\partial u}{\partial x}\right) + s(x)\right] dx + [uv]_0^{b(t)} \\ &= u^m \frac{du}{dx} + uv\Big|_0^{b(t)} + \int_0^{b(t)} s(x)\,dx \\ &= u(b)\,\dot{b} - u(b)^{m-1}\frac{\partial u(b,t)}{\partial x} + \frac{db}{dt} + \int_0^{b(t)} s(x)\,dx \end{aligned} \tag{3.30}$$

$$= \int_0^{b(t)} s(x)\,dx \tag{3.31}$$

since the first term of (3.30) vanishes by virtue of the zero total flux boundary condition in (2.16).

Although local mass cannot be conserved, the integral of u in the segment from 0 to

$\hat{x}_i(t)$ can be assumed to be a constant fraction of (t), so the following mass fractions integral $_i$:

$$\frac{1}{(t)} \int_0^{\hat{x}_i(t)} u\,dx = {}_i \tag{3.32}$$

is constant for all time. Note that $_N = 1$.

We approach conservation of $_i$ in a similar fashion as for the c_i in §3.1.1. We begin by multiplying both sides of (3.32) by (t) and taking the time derivative of the resulting equation so that

$$\begin{aligned} \frac{d}{dt} \int_0^{\hat{x}_i(t)} u\,dx &= \frac{d}{dt}\left((t)\ {}_i \right) \\ &= {}^0(t)\ {}_i \end{aligned} \tag{3.33}$$

Evaluating the left hand side of (3.33), it can be shown in a similar manner as for (3.30) that

$$\frac{d}{dt} \int_0^{\hat{x}_i(t)} u\,dx = u(\hat{x}) \quad u(\hat{x})^{m\ 1} \frac{@u(\hat{x})}{@x} + \frac{d\hat{x}}{dt} \quad + \int_0^{\hat{x}_i(t)} s(x)dx$$

Now substituting (3.31), (3.32) and (3.34) into (3.33) we can rearrange to find the nodal velocity

$$\frac{d\hat{x}}{dt} = \frac{\int_0^{b(t)} s(x)dx \quad (\hat{x})}{u(\hat{x})} \quad u(\hat{x})^{m\ 1} \frac{@u(\hat{x})}{@x} \quad \frac{1}{u(\hat{x})} \int_0^{\hat{x}_i(t)} s(x)dx \tag{3.34}$$

which consists of the Darcy velocity (3.5), together with a contribution from the source term. As in §3.1, we can employ explicit Euler timestepping for $\hat{x}_i(t)$ or use semi-implicit timestepping, although the latter requires the terms in (3.34) to be written as a derivative.

Conservation of partial mass in each segment tells us that the $_i$'s in (3.32) remain constant in time, therefore for a general point $\hat{x}_i(t)$

$${}_i = \frac{\int_{\hat{x}_{i-1}(t^{n+1})}^{\hat{x}_{i+1}(t^{n+1})} u(x;t^{n+1})dx}{\int_0^{b(t^{n+1})} u(x;t^{n+1})dx} = \frac{\int_{\hat{x}_{i-1}(t^0)}^{\hat{x}_{i+1}(t^0)} u(x;t^0)dx}{\int_0^{b(t^0)} u(x;t^0)dx} \tag{3.35}$$

allowing us to nd the solution u

Substituting in (3.37) we have

$$\begin{aligned}
{}^{0}(t) &= \int_0^{b(t)} r^{d-1}\left[\frac{1}{r^{d-1}}\frac{@}{@r}\left(r^{d-1}u^m\frac{@u}{@r}\right) + r^{d-1}s(r)\right]dr + \left[ur^{d-1}v\right]_0^{b(t)} \\
&= r^{d-1}u^m\frac{@u}{@r} + ur^{d-1}v\Big|_0^{b(t)} + \int_0^{b(t)} s(r)dr \\
&= u(b)r(b)^{d-1} - u(b)^{m-1}\frac{@u(b)}{@r} + \frac{db}{dt} + \int_0^{b(t)} s(r)r^{d-1}dr \qquad (3.39) \\
&= \int_0^{b(t)} s(r)r^{d-1}dr \qquad (3.40)
\end{aligned}$$

where the first term of (3.39) vanishes by the zero flux boundary condition in (2.16).

The integral of u from 0 to $r_i(t)$ is now assumed to be a constant fraction of (t) so the following mass fraction integral $_i$:

$$\frac{1}{(t)}\int_0^{r_i(t)} ur^{d-1}dr = {}_i \qquad (3.41)$$

is constant for all time.

We approach the conservation of $_i$ as we did in x3.2.1, except for the radial case. We begin by multiplying both sides of (3.41) by (t) and then taking the time derivative of the resulting equation so that

$$\begin{aligned}
\frac{d}{dt}\int_0^{r_i(t)} udr &= \frac{d}{dt}\left((t) {}_i\right) \qquad (3.42) \\
&= {}^{0}(t) {}_i \qquad (3.43)
\end{aligned}$$

Evaluating the left hand side of this, for a general point $r_i(t)$ it can be shown in a similar manner as for (3.39) that

$$\frac{d}{dt}\int_0^{r_i(t)} ur^{d-1}dr = u(r_i)r_i - u(r_i)^{m-1}\frac{@u(r_i)}{@r} + \frac{dr_i}{dt} + \int_0^{r_i(t)} s(r)r^{d-1}dr \qquad (3.44)$$

Now substituting (3.40), (3.41) and (3.44) into (3.42) we can rearrange to find the nodal velocity

$$\frac{dr_i}{dt} = \frac{\int_0^{b(t)} s(r)r^{d-1}dr - (r_i)}{r_i^{d-1}u(r_i)} - u(r_i)^{m-1}\frac{@u(r_i)}{@r} - \frac{1}{r_i u(r_i)}\int_0^{r_i(t)^{d-1}} s(r)r^{d-1}dr \qquad (3.45)$$

which as in x3.2.1 consisits of the Darcy velocity together with other terms due to the source. We can therefore employ the same timestepping methods as for (3.34) to recover the new mesh spacing.

Due to the conservation of partial mass in each section we can use the new mesh spacing to recover the solution u. We apply a mid-point rule to (3.41) to give

$$u_i(r;t^{n+1}) = \frac{(t^{n+1})}{r_i^{d-1}(t^{n+1})\,(r_{i+1}(t^{n+1}) - r_{i-1}(t^{n+1}))} \qquad (3.46)$$

where $(t^{n+1}) = (t^n) + t\,{}^0(t^{n+1})$ and ${}^0(t^{n+1})$ can be found directly after each redistribution of nodes using (3.40).

3.3 The Finite Difference Algorithm

Without loss of generality, we write the algorithms for Cartesian coordinates, as it is a trivial change to use radial coordinates. We shall be solving this problem on a mesh x_i, for $i = 0;:::N$, such that

$$a(t) = x_0(t) < x_1(t) < ::: < x_{N-1}(t) < x_N(t) = b(t) \qquad (3.47)$$

with moving boundaries at a(t) and b(t), where the movement of $x_i(t)$ is caused by the

2. Compute the nodal velocity as in x3.1.1. (If using the semi-implicit method as in x3.1.3 skip to step 4.)

3. Compute the updated mesh using

$$x_i^{n+1} = x_i^n + \quad t v_i \tag{3.49}$$

where t is the time-step.

4. Recover the new mass distribution as described in x3.1.2 using the initial masses c_i^0 found in step one of this algorithm.

5. Repeat previous three steps for chosen number of time steps

3.3.2 [illegible]

Given the mesh $x_i(t^0)$ and solution $u(x_i; t^0)$ at initial time t_0, the algorithm is:

1. Compute the initial total mass (t^0)

$$(t^0) = \int_0^{b(t^0)} u^0 dx \tag{3.50}$$

and also the initial partial masses

$$c_i^0 = \int_0^{x_i(t^0)} u^0 dx \tag{3.51}$$

and then compute the mass fractions $_i$

$$_i = \frac{\int_0^{x_i(t^0)} u^0 dx}{\int_0^{b(t^0)} u^0 dx} \tag{3.52}$$

2. Compute the nodal velocity as in (3.34).

3. Compute the updated mesh using

$$x_i^{n+1} = x_i^n + \quad t v_i : \tag{3.53}$$

and the new total mass

$$^{n+1} = \ ^n + \quad t \ (\ ^0)^n \tag{3.54}$$

4. With the new partial mass

$$c_i = {}_i{}^{n+1} \tag{3.55}$$

recover the new mass distribution, using (3.36), with the partial mass fractions ${}_i$'s found in step one of this algorithm.

5. Repeat previous four steps for chosen number of timesteps

Chapter 4

Finite element formulation

In this chapter we describe a finite element approach to deriving a moving mesh method for the PME. As in the previous chapter we describe the method based on the assumption of local mass conservation (consistent with the total integral of density being constant). The method will firstly be used to find the velocity of nodes in the non-evaporation case where conservation applies, and then in the evaporation case where conservation no longer applies.

The finite element formulation combines a particular finite representation of the solution u with a weak form of the PME. To implement this we introduce a weak form of the conservation principle using a continuous and once-differentiable test function w_i for $(0 \quad i \quad N)$ advected with the mesh velocity v. We define a distributed mass c_i as

$$\int_0^{b(t)} w_i u \, dx = c_i \tag{4.1}$$

for $(0 \quad i \quad N)$.

So as not to alter the total mass of the problem we require the w_i's to be a partition of unity, so that

$$\sum_{j=0}^{N} w_j = 1 \tag{4.2}$$

Here we choose w to be a standard piecewise linear nite element hat function $_i$ where

$$_i = \begin{cases} \frac{x_{i+1} \quad x}{x_{i+1} \quad x_i} & \text{if } x \; 2 \; (x_i ; x_{i+1}); \\ \frac{x \quad x_{i \quad 1}}{x_i \quad x_{i \quad 1}} & \text{if } x \; 2 \; (x_{i \quad 1}; x_i); \\ 0 & \text{otherwise:} \end{cases} \tag{4.3}$$

for (2 i N 1) (with suitable modi cations at $i = 0; N$), which agrees with the condition (4.2) enforced upon w whilst at the same time providing useful compact support. The solution u is a linear combination of the basis functions (4.3).

4.1 Dig ybo a

4.1.1 1D eeh n

We now propose a mass conservation principle in which the distributed mass c_i will remain constant for all time. As in x3.1.1, to get the velocity we di erentiate the mass and apply Leibnitz' Integral rule to (4.1) so that

$$\frac{d}{dt} \quad Z_{b(}$$

dimensional Cartesian PME (2.14),

$$\frac{d}{dt}\left(\int_0^{b(t)} {}_i u\,dx\right) = \int_0^{b(t)} {}_i \left[\frac{\partial}{\partial x}\left(u^m \frac{\partial u}{\partial x}\right) + \frac{\partial (uv)}{\partial x}\right] dx = 0 \tag{4.6}$$

Integrating (4.6) by parts we find

$$\int_0^{b(t)} {}_i \left[\frac{\partial}{\partial x}\left(u^m \frac{\partial u}{\partial x}\right) + \frac{\partial (uv)}{\partial x}\right] dx = {}_i \left[u^m \frac{\partial u}{\partial x} + uv\right]_0^{b(t)}$$

$$- \int_0^{b(t)} \frac{\partial {}_i}{\partial x}\left(u^m \frac{\partial u}{\partial x}\right) + (uv)\, dx \tag{4.7}$$

$$= - \int_0^{b(t)} \frac{\partial {}_i}{\partial x}\left(u^m \frac{\partial u}{\partial x}\right) + (uv)\, dx \tag{4.8}$$

$$= 0; \tag{4.9}$$

for (0 i N

As we can see from the K matrix entries, we have averaged u across the nodes. This is because it is a linear function of x.

Imposing

which results in the matrix system

$$M\underline{u} = \underline{c} \tag{4.23}$$

where M is a non-singular mass matrix and $\underline{c}$ is a vector of c_i's which can be pre-computed at $t = t_0$, that we can solve for (4.22). Hence

$$\underline{u} = M^{-1}\underline{c} \tag{4.24}$$

The coefficient matrix M is tridiagonal of the form

$$M = \begin{pmatrix} M_{0;0} & M_{0;1} & 0 & \cdots & \cdots & \cdots & 0 \\ M_{1;0} & M_{1;1} & M_{1;2} & 0 & & & \vdots \\ 0 & \ddots & \ddots & \ddots & & & \vdots \\ \vdots & & M_{i;i-1} & M_{i;i} & M_{i;i+1} & & \vdots \\ \vdots & & & \ddots & \ddots & \ddots & 0 \\ \vdots & & & & M_{N-1;N-2} & M_{N-1;N-1} & M_{N-1;N} \\ 0 & \cdots & \cdots & \cdots & 0 & M_{N;N-1} & M_{N;N} \end{pmatrix}.$$

begin with the total mass

$$\int_0^{b(t)} u\,dx = \Gamma(t); \tag{4.25}$$

which varies with time. The derivative of (4.25) has already been shown in x3.2.1 to be

$$\Gamma' = \int_0^{b(t)} s(x)\,dx \tag{4.26}$$

We also de ne the distributed mass from 0 to b(t) as

$$\int_0^{b(t)} \rho_i u\,dx \tag{4.27}$$

We express the distributed mass as a fraction of the total mass to give

$$\frac{1}{\Gamma(t)} \int_0^{b(t)} \rho_i u\,dx = \rho_i \tag{4.28}$$

which we assume to be constant in time. Now multiplying both sides of (4.28) by $\Gamma(t)$ and taking the time derivative we have

t

$$\frac{d}{dt} \int_0^{b(t)} \rho_i u\,dx = \rho_i \Gamma'(t) \tag{4.29}$$

where we have used the zero ux boundary condition from (2.16).

Putting this all together into (4.29), we rearrange to make the velocity term the subject giving

$$\int_0^{b(t)} \frac{\partial_i}{\partial x} uv\,dx = \left[\int_0^{b(t)} s(x)\,dx \right]_0^{b(t)} \int_0^{b(t)} \frac{\partial_i}{\partial x} u^m \left(\frac{\partial u}{\partial x} \int_0^{b(t)} s(x)\,dx \right) dx + \int_0^{b(t)} s(x)\,dx \tag{4.34}$$

We can treat this in an almost identical way, as we did (4.10), the only di erence being the right hand side which we now call $\underline{f}$. Once again we write the velocity as the derivative of the velocity potential and solve the matrix system

$$K\underline{\ } = \underline{f} \tag{4.35}$$

from which we nd the velocity potentials . As in x4.1.1 we can di erentiate to nd the velocity and then interpolate, using equation (4.20), to recover v at the nodes.

4.2.2 igeb u thm

As in x4.1.2 the solution u can be recovered directly from the nite element form. Since the $_i$'s are constant for all time we have

$$_i = \frac{1}{(t)} \int_0^{b(t)} {}_i(x)u(x)\,dx = \left[\frac{1}{(t)} \int_0^{b(t)} {}_i(x)u(x)\,dx \right]_{t=t_0} \tag{4.36}$$

As in x4.1.2 we expand u(x) in terms of the basis function and the partial mass at time t from (4.36) becomes

$$\frac{1}{(t)} \int_0^{b(t)} {}_i u\,dx = \int_0^{b(t)} {}_i(x) \sum_{j=0}^{N} u_j \, {}_j(x)\,dx \tag{4.37}$$

$$= \sum_{j=0}^{N} \int_0^{b(t)} {}_i(x) \, {}_j(x)\,dx u_j = {}_i \tag{4.38}$$

This results in the non-singular matrix system

$$M\underline{u} = \underline{d} \tag{4.39}$$

$$) \quad \underline{u} = M^{1}\underline{d}$$

4. Compute the new solution by solving the matrix system (4.24) where the right hand side can be computed using the c_i's from step 1.

5. Repeat the previous four steps for the chosen number of time steps.

4.3.2 [illegible]

Given the mesh and solution at initial time t^0, the algorithm is:

1. Compute the initial total mass (t^0)

$$\int_0^{b(t^0)} u^0 dx = (t^0) \tag{4.43}$$

the weak form of the initial masses d_i

$$\int_0^{x_i(t^0)} {}_i u^0 dx = d_i : \tag{4.44}$$

and the mass fractions $_i$

$$_i = \frac{\int_0^{b(t^0)} {}_i u^0 dx}{\int_0^{b(t^0)} u^0 dx} \tag{4.45}$$

2. Compute the nodal velocitys from the velocity potentials as described in x4.2.1.

3. Compute the updated mesh using

$$x_i^{n+1} = x_i^n + t v_i : \tag{4.46}$$

Use the new mesh distribution to calculate $^0(t^{n+1})$ directly from (4.26) and from this the new total mass

$$(t^{n+1}) = (t^n) + t \, ^0(t^{n+1}) \tag{4.47}$$

4. Use the new total mass (4.47) to recover the solution u as described in x4.2.2.

5. Repeat the previous four steps for the chosen number of time steps.

Chapter 5

Results

We split the results chapter into two main sections. We begin by presenting numerical results for the methods described in Chapter 3 and Chapter 4, followed by a comparison of the numerical model with some real data.

5.1 Methods

We first describe numerical results for the methods derived in Chapter 3 and Chapter 4. We pay particular attention to the differences between fast diffusion and slow diffusion and also the effects of evaporation. Since the various methods described provide similar results we do not show them all for each one. Instead we display results for chosen cases, illustrating the various methods described.

We begin by comparing results for fast diffusion and slow diffusion using the mass conserving 1D finite element model derived in §4.1. We analyse several plots that have been produced to give good supporting arguments to our observations, allowing us to deduce the various behaviour.

We then investigate the effects of evaporation on the two dimensional radially symmetric PME for both the fast and slow diffusive regimes. We show that we can force

retreat of the boundary in both cases.

5.1.1 [illegible]

To run the numerical model we need to de ne boundary conditions and initial data.

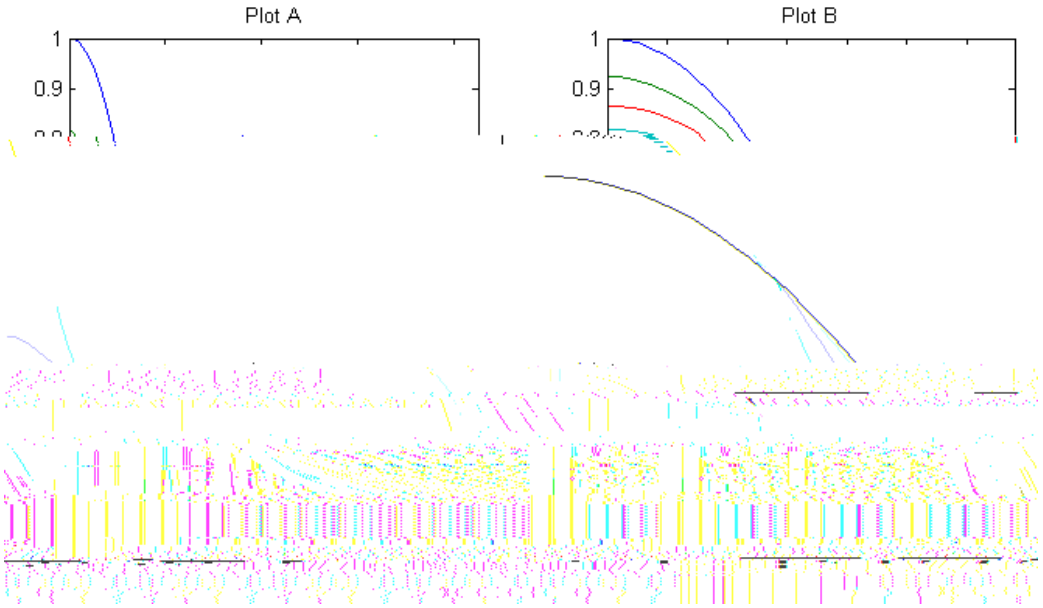
Plot A
1
0.9
Plot B
1
0.9

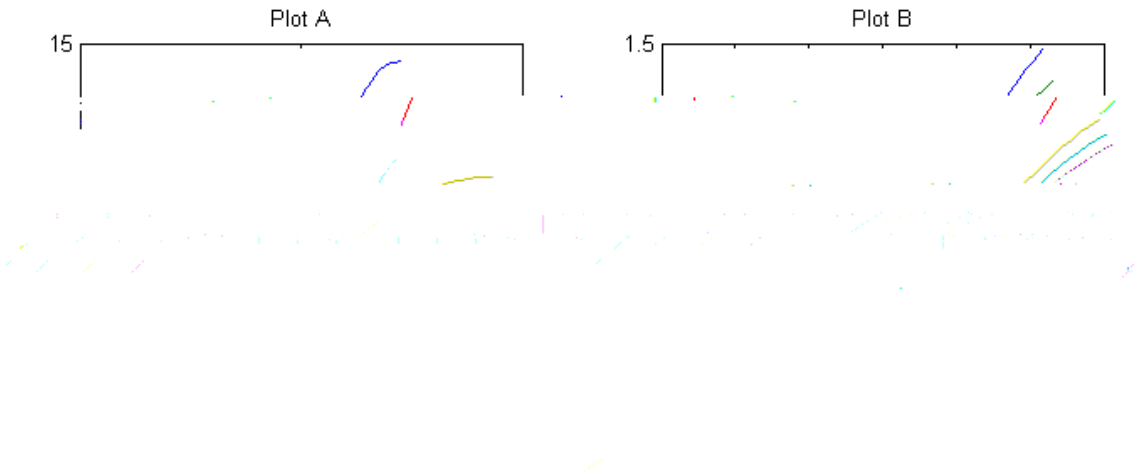

Figure 5.2: Velocities of the nodes for numerical solutions of the PME with Plot A: m = 1:5, Plot B: m = 1

imately one order of magnitude di erence between the velocities of the nodes between the two regimes, explaining how fast the mass spreads for the fast di usive regime. We also see that for the slow di usive regime the distribution between the variables is almost linear, which supports the idea of little deformation occuring from the initial spread. For the fast di usive regime the nodes close to the boundary are moving much faster than those near the origin, displayed by the attening of the distributions near the boundary positions in Plot A. This supports the idea of larger deformation from the initial data. A further key di erence is that the velocities for the fast di usive regime are decreasing a signi cant amount more than those for slow di usion, implying that the fast di usion process is more powerful initially but tends towards a more similar rate. A nal interesting observation for gure 5.2 is that the velocities for fast di usion keep a similar form throughout the time that the model is run for. This contradicts what was observed in 5.1 where the distribution appeared to initially change from the initial distribution and then return to a similar form.

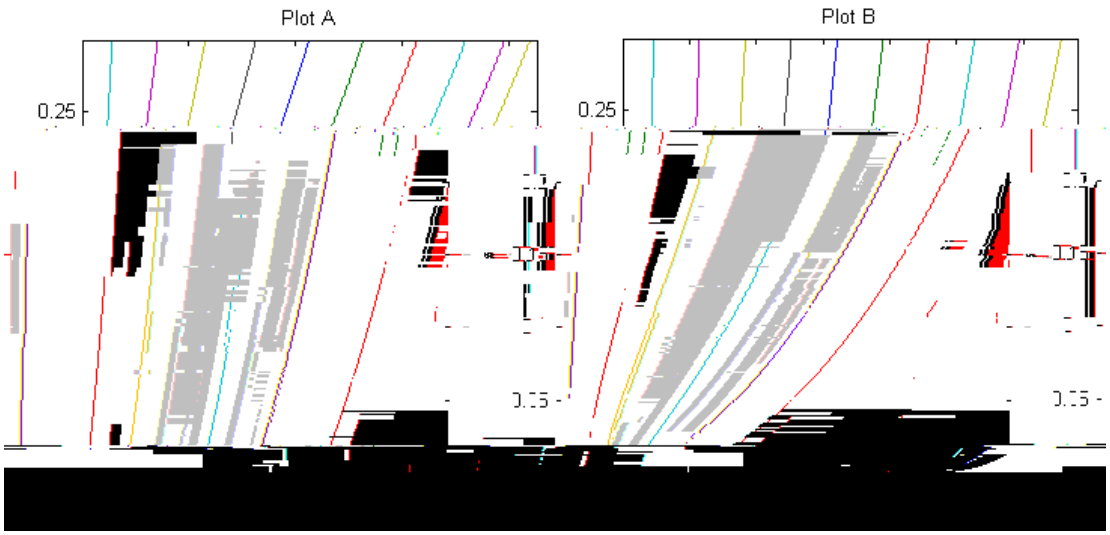

Figure 5.3: Trajectories of the nodes for the numerical solutions of the PME with Plot A: m = 1:5, Plot B: m = 1

Finially, gure 5.3 shows the trajectories of the nodes from gure 5.1. We see that for the fast di usive regime, because of the increasing nodal velocities, as we get towards the free moving boundary of u, the distribution initially spreads at a very high rate compared with that of slow di usion which, as would be expected from Plot B of gure 5.2, stays almost linear. However by the end of the time period Plot A shows that the nodal speed is rapidly decreasing as the gradient appears to tend towards that of Plot B, agreeing with similarities between later distributions in gure 5.1.

The results displayed in this section are all consistent with what we would expect from the PME in the fast di usion regime, since it contains u^m which becomes large when $m < 0$ and u is small. (We note that the magnitude of m taken, 1:5 for fast di usion, is not too large as to trigger superfast di usion [16])

5.1.3 E e ts of evaporation

We now take a look at the e ects of evaporation on the 2D radially symmetric PME with a source term ((3.37) with d = 2) for both the fast and slow di usive regimes.

(Ideally this would be modelled in 3D, however as mentioned in x3.2.2 this cannot be done in the radially symmetric case since the evaporation only occurs at the boundary which wouldn't be taken into account in the model developed here.)

We plot the elapsed time against the position of the free moving boundary $r(N)$ for both fast and slow di usion.

the fast di usive regime also appears to amplify the e ect of the source term. After reaching it's peak distance at a later time, the boundary in Plot A recedes around 0:17 spacial units as opposed to around 0:08 spacial units in Plot B.

If we choose the value of s(r) to be too large the distribution of mass falls below the boundary u = 0:1 just before the leading edge. This behaviour is unphysical in the context of the prroblem described in x1.1. This is because we chose our boundary conditions and initial data x5.1.1 based on there being a limit at this point, beyond which the liquid capillary network bridges are no longer connected.

5.2 Tehp

We now compare the numerical results to some experimental data. This will give us an idea of how accurately the models work in a particular application. This particular example is representative of those described by the aims set out in x1.1.

The experimental data from the University of Santa Barbara [12] is for liquid spreading of TEHP, which is an organophosphate liquid with low vapour pressure at room temperatures. This means that the evaporation e ects will be negligable in this case.

The liquid begins on the surface of the porous medium. Once it has di used into the medium, only at saturation levels below around 20% can we start to consider the fast di usion process [12]. We would then expect the geometry to be hemispherical, therefore the most appropriate model we have to compare to experimental data is the one described in x3.1.4 for the radially symmetric PME (3.16) with d = 3.

Since the received data has dimensions, we take the PME in the appropriate form, using the derivation in x2.1 and non-dimensionalise it. By doing this we can compare numerical results produced by the program to the non-dimensional experimental results

quantitavely. We begin with the 3D radially symmetric PME in the form

$$\frac{@S}{@t} = D_0 \frac{1}{r^2} \frac{@}{@r} \left(\frac{r^2}{(S - S_0)^m} \frac{@S}{@r} \right) \tag{5.3}$$

where S is the saturation measured as a percentage of full saturation, S_0 is taken to be a fraction of the boundary value and D_0 is the di usion coe cient with units $m^2 s^{-1}$.

The given data provides the volume in (m^3) of the saturated area, which by the hemispheric geometry gives the position of the boundary, i.e. the radius as

$$R = \left(\frac{3V_0}{2} \right)^{\frac{1}{2}} \tag{5.4}$$

We would like (5.3) in a similar form as (3.16) so we de ne the non-dimensional variables t' and r' such that

$$r' = \frac{r}{R_0}; \qquad t' = t$$

porous grain particles will break and the model no longer applies. The value Smax is the highest level of saturation from the data set. From (5.8), the factor (Smax S(b)) in front of the cosine function is equivalent to k from (2.17). The results are as follows:

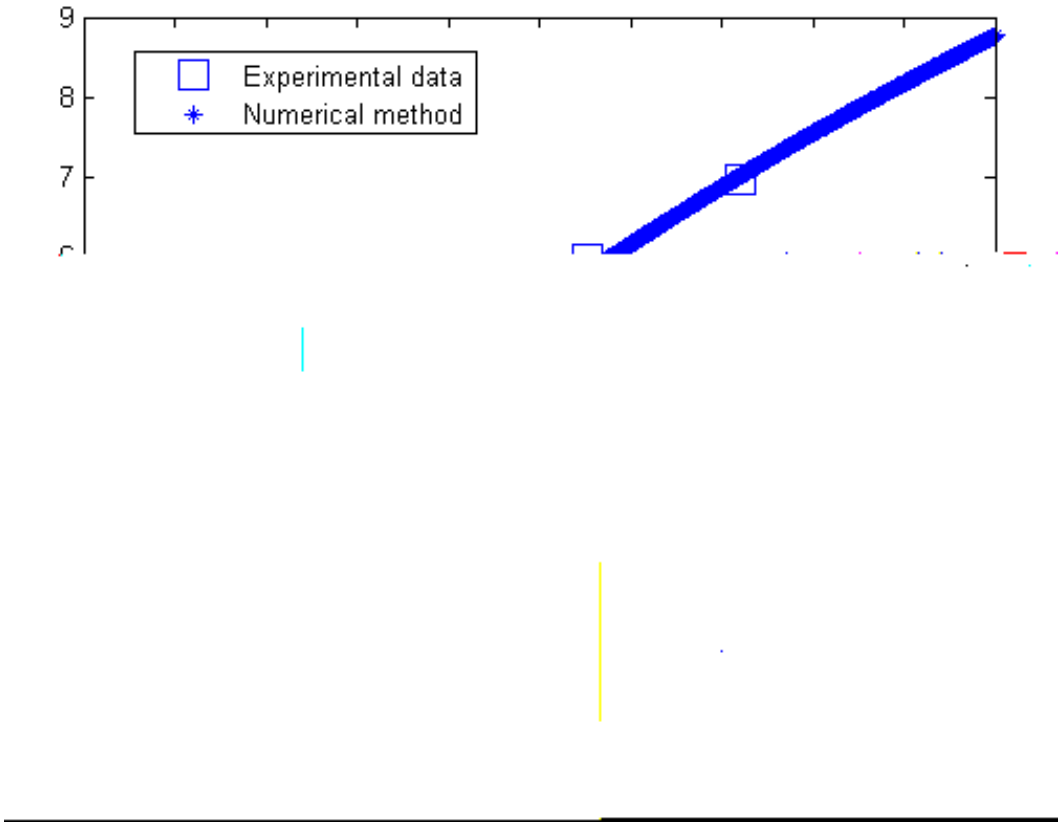

Figure 5.5: Numerical solutions of the radiall symmetric 3D PME plotted against values from experimental data.

From gure 5.5 we see that there is a very good match between the numerical method output and the experimental values. Therefore for this data set we can conclude that the model provides a good representation for fast di usion in porous media.

Chapter 6

Conclusions and Future Work

In this final chapter we summarise the work carried out in this project, followed by ideas for future development in this area of research.

6.1 Summary

In this dissertation we have looked at a variety of ways in which to use a velocity based moving mesh method to model both fast and slow diffusion in a porous medium. In particular, we have implemented such a numerical method in various geometries for the fast diffusion process and found a strong correlation between the output produced and experimental data modelling a chemical agent diffusing in a porous substrate under similar conditions.

We worked throughout the project on a one-dimensional domain. In Chapter 3 we began by formulating a velocity based moving mesh method based on the principle of local mass conservation, in order to model the evolution of the PME in time. This was done in both 1D Cartesian coordinates and also in d-dimensional radially symmetric coordinates. The advantage of the radially symmetric coordinates was that we could

model 3D spherical phenomenon in 1D, making the later comparison with experimental results possible. Using the same coordinate systems we then modelled the PME with a source term to represent evaporation happening within the domain under the principles of conservation of mass fractions.

In Chapter 4 we followed up the work from the previous chapter by deriving a nite element formulation of the problem. This used a similar methodology with a velocity based moving mesh method employed for both the mass conserving and evaporative situations. This was modelled in 1D Cartesian coordinates. Had it not been for time constraints the model would have been moved into higher dimensions. It would have been of particular interest to be able to extend the model to 3D nite elements, since this would have provided the opportunity to model the evaportation process at the boundaries of a 3D domain. The model output could then have been compared to the appropriate experimental data, further developing the framework of applications to be considered.

In Chapter 5 we discussed the results, which were split into two main sections. We began from a mathematical modelling standpoint by using the various models to compare the fast and slow di usive regimes, followed by comparisons between the e ects of incoorporating evaporation into both of these cases.

Finally we looked at results from an experimental point of view. We ran the most appropriate model with some conditions imparted by experimental data from [12] and compared the output of the numerical model to the normalised experimental data.

fast di usion in porous media, in general geometries.

6.2 Fture work

To complement this dissertation we now suggest some ideas for future development in this area.

Evaporation

Currently, outside this dissertation there is apparantly no work within this application of how to model evaporation mathematically. Ideally the next development in this eld would be to accurately model this process. However this poses several di cul-

concerning wet granular systems. Drying and separation of granular molecules can have catastrophic e ects such as causing landslides and avalanches.

In the study of the dynamics of wet granular matter knowledge of the levels of saturation within a porous material is highly important. In [11] it is described how dry sand acts as if it were in a liquid state, whereas saturated sand can be formed into reasonably stable structures. A particular example is presented in [11] of a large landslide where a part of the slope has moved downwards and has left a parabola shape in the remaining earth, implying that it was in a viscous liquid state as it fell. A further observation is that the adjacent parts of the land where conditions would most likely be similar nothing has happened. This could imply that this is a threshold process whereby if the saturation of soil falls below a certain level then it reaches a liquid state.

In the study of avalanches, as described in [10], the water saturation of natural snow cover varies. The snow acts as a porous medium and in general water lls up to 20% of the pore volume. When the saturation level is around 7%, we enter the fast di usion regime. Saturation below this level can be critical as the bridges between pores might break causing the snow granules to part. On a large scale this could cause an avalanche.

Since the two previous examples include much larger height scales and masses than in the chemical agents problem, when formulating a model for these processes we

2D and 3D Finite Element Method

The natural progression in a modelling sense would be to attempt to increase the Catesian coordinate spatial dimensions for the finite element method. We suggest this approach rather than finite differences because, in general for curved boundaries, the finite element method provides a better approximation to the solution. Modelling with 2D finite elements was close to being put into practice for this project and would have provided a good addition to the current framework.

for the 1D cartesian version and see [3] for the 1D radially symmetric version. However these would not have been useful in the fast di usive regime, which is another reason why similarity solutions have not been followed up in this dissertation.

We nally consider two ways in which to adjust the mesh being used.

In order to increase the accuracy of the moving mesh method, the initial mesh can be altered. One way is to create an optimal initial mesh as in [1]. This essentially adjusts the initial distribution of the mesh so as to minimize the L_2 norm of the di erence between the approximation to the initial conditions to and the exact initial function over the mesh values.

Another reason to alter the initial mesh is when higher resolution is required in a particular part of the solution. One way in which this can be done is by using equidistribution which relocates grid points without increasing the total number of them. Altering the initial mesh in this way could be useful for example, when tracking a moving boundary by increasing the resolution near the boundary.

,

B

[1] M. Baines, Algorithms for optimal discontinuous piecewise linear and constant l_2 ts to continuous functions with adjustable nodes in one and two dimensions, Mathematics Of Computation, 62 (1994), pp. 645{669.

[2] M. Baines, M. Hubbard, and P. Jimack, A moving mesh nite element algorithm for the adaptive solution of time-dependent partial differential equations with proportional recovery, Applied Numerical Mathematics, 27(6Numer.]326(p
M05012011051, pp. 65091(o{576)]TJ -18.21 -30.778 Td [([24)]TJ/F19 11.9552 Tf

[9] W. Cao, W.Z.Huang, and R. Russell, A moving-mesh method based on the geometric conservation law, SIAM J. Sci. Comput., 24 (2002), pp. 118–142.

[10] A. Denoth, Wet snow pendular regime: the amount of water in ring-shaped configurations, Cold Regions Science and Technology, 30 (1999), pp. 13–18.

[11] S. Herminghaus, Dynamics of wet granular matter, Advances in Physics, 54 (2005), pp. 221–261.

[12] A. Lukyanov, Private communication, 2011.

[13] K. Morton and D. Mayers, Numerical Solution of Partial Differential Equations, Cambridge University Press, 1994.

[14] K. Osman, MSc thesis: Numerical schemes for a non-linear diffusion problem, msc dissertation